

This is an electronic reprint of the original article. This reprint may differ from the original in pagination and typographic detail.

Effect of Return Fines Embedding on the Sintering Behaviour of Vanadium Titanium Magnetite Concentrates

Peng, Shihong; Liu, Hao; Hua, Huangjie; Sun, Zezheng; Qin, Yuelin; Meng, Fei; Liu, Weiqiang; Wang, Guang

Published in:
Metals

DOI:
[10.3390/met13010062](https://doi.org/10.3390/met13010062)

Published: 01/01/2023

Document Version
Final published version

Document License
CC BY

[Link to publication](#)

Please cite the original version:

Peng, S., Liu, H., Hua, H., Sun, Z., Qin, Y., Meng, F., Liu, W., & Wang, G. (2023). Effect of Return Fines Embedding on the Sintering Behaviour of Vanadium Titanium Magnetite Concentrates. *Metals*, 13(1), Article 62. <https://doi.org/10.3390/met13010062>

General rights




Copyright and moral rights for the publications made accessible in the public portal are retained by the authors and/or other copyright owners and it is a condition of accessing publications that users recognise and abide by the legal requirements associated with these rights.

Take down policy

If you believe that this document breaches copyright please contact us providing details, and we will remove access to the work immediately and investigate your claim.

Article

Effect of Return Fines Embedding on the Sintering Behaviour of Vanadium Titanium Magnetite Concentrates

Shihong Peng ¹, Hao Liu ^{1,*}, Huangjie Hua ¹, Zezheng Sun ¹, Yuelin Qin ¹, Fei Meng ¹, Weiqiang Liu ² and Guang Wang ³

¹ School of Metallurgy and Materials Engineering, Chongqing University of Science and Technology, Chongqing 401331, China

² Process and Systems Engineering Laboratory, Faculty of Science and Engineering, Åbo Akademi University, FI 20500 Åbo, Finland

³ Department of Materials Science and Engineering, McMaster University, 1280 Main Street West, Hamilton, ON L8S 4L7, Canada

* Correspondence: liuhao@cqust.edu.cn; Tel.: +86-135-0831-9393

Abstract: To improve the permeability of sinter packed bed for achieving the efficient utilization of low-grade iron bearing minerals, the effect of the returned fines embedding on productivity, yield, flame front speed (FFS) in the vanadium titanium magnetite (VTM) sintering process, tumble index (TI) of sinter, and permeability of the sinter packed bed was clarified. Results indicate that the productivity, yield, flame front speed, and tumble index of the vanadium titanium magnetite sintering process are all increased to a certain extent after embedding different sizes of returned fines, and the optimal sintering indices occur when the particle size of return fines for embedding is 3–5 mm. The optimal mass ratio of return fines for embedding was confirmed at 80%, and a continued increase in the mass ratio results in a decrease in flame front speed, yield, productivity, and tumble strength. Among the five different possible locations of embedded return fine layer, the middle-lower layer corresponds to the highest flame front speed. As the mass ratio of return fines for embedding is enhanced from 0% to 50%, the permeability of the sinter packed bed is improved at each stage of sintering.

Keywords: sinter; return fines embedding; vanadium titanium magnetite; sintering behavior



Citation: Peng, S.; Liu, H.; Hua, H.; Sun, Z.; Qin, Y.; Meng, F.; Liu, W.; Wang, G. Effect of Return Fines Embedding on the Sintering Behaviour of Vanadium Titanium Magnetite Concentrates. *Metals* **2023**, *13*, 62. <https://doi.org/10.3390/met13010062>

Academic Editor: Felix A. Lopez

Received: 25 November 2022

Revised: 14 December 2022

Accepted: 20 December 2022

Published: 26 December 2022



Copyright: © 2022 by the authors. Licensee MDPI, Basel, Switzerland. This article is an open access article distributed under the terms and conditions of the Creative Commons Attribution (CC BY) license (<https://creativecommons.org/licenses/by/4.0/>).

1. Introduction

As an important mineral resource, Vanadium titanium magnetite (VTM) has a high comprehensive utilization value due to it containing abundant high-value elements such as vanadium and titanium [1]. It is usually used as the iron-containing raw material for sintering process. During sintering, raw materials, including fluxes, fuel, iron ores, and their return fines, are blended according to certain proportion and then granulated primarily to produce granules with proper size, and strength, as well as desired components [2]. The proper size distribution and strength of granules is conducive to achieve the ideal sinter bed permeability. The permeability of the sinter packed bed would significantly influence the flame front travelling speed and the heat transformation during the sintering process, which in turn determines the sinter productivity, yield and quality [3]. For the VTM sintering process, the small specific surface area and poor hydrophilicity of VTM lead to undesirable granulation performances [4], which adversely affects the bed permeability. Moreover, VTM sinter has poorer metallurgical properties and strength compared with conventional sinter due to the rich content of TiO₂ in mineral components. Thus, for the VTM sintering, high bed permeability is especially meaningful.

To improve the permeability of sinter packed bed for achieving efficient utilization of low-grade iron bearing minerals, extensive studies have been reported worldwide. The most effective way to obtain the desired permeability of a sinter packed bed is to enhance

the granulation properties of the granules, which includes using an intensive mixing machine [5–10] and the addition of solid binder [11–15] in the granulation. In addition to this, the optimized moisture [16–20] and the implementation of pre-briquetting treatment [21] in the granulation process also improve granulation performance. For example, Ji et al. [8] investigated the influence of intensive mixing methods on granulation and found that compared to conventional mixing, the permeability improved from 7.32 JPU to 10.32 JPU at 9.0% moisture with intensive mixing. Zhang et al. [13] found that the addition of burnt lime and bentonite could significantly improve the bed permeability. A 2% burnt lime and 1.2% bentonite addition level could increase the bed permeability from 48.77 JPU to 61.42 JPU and 53.93 JPU to 64.97 JPU respectively. Meanwhile, Zhou et al. [22] revealed that the 2% addition of hydrated lime can distinctly reduce granule degradation and then improve permeability from 40.45 JPU to 46.05 JPU at 7.7 wt% granulation moisture. Lv et al. [23] proposed a prewetting granulation technology and found that the bed permeability of granules raised approximately 0.25 times by optimizing the amount of water on the surfaces of different particles via prewetting treatment. Zhu et al. [21] found that the permeability of green mixture prepared by the pre-briquetting sintering process is higher than that of the traditional sinter process in approximately 8 JPU.

There are many existing methods to elevate the permeability of the sinter packed bed. For example, return fines embedding technology was proposed by Kasai et al. [24,25] which can control the formation of the void structure in the sinter cake. In addition, a wall effect at the vicinity of the pellet surface is helpful to enhance the permeability of the sinter packed bed. After that, Matsumura et al. [26] investigated the effect of the mass ratio of return fines embedded in the sinter packed bed on productivity, flame front speed (FFS), and yield. They found that with the increase of mass ratio of return fine for embedding, productivity and FFS are increased, but the yield is decreased with enhancing FFS. Moreover, they applied return fines embedding technology to three sinter plants, which revealed that return fines embedding technology could considerably improve productivity. Wang et al. [27] also found that with applying return fines embedding technology, the FFS and productivity were raised from 21.66 mm/min and 1.46 t/(m²·h) to 23.86 mm/min and 1.54 t/(m²·h) respectively. Liu et al. [28] studied the effect of different particle sizes and mass ratios for return fines embedding on the sintering process. They found that the productivity was higher when the size of return fines for embedding was larger than 1 mm, and the strength of sinter was also bigger when the size of return fines was larger than 3 mm. In addition, when the mass ratio of returned fines for embedding was 25%, the productivity increased by 2.8%.

The investigators have conducted research on the effect of return fines embedding on the sinter packed bed permeability, productivity, FFS, and cold strength. Similarly, numerous studies have been conducted to improve the properties and productivity of VTM sinter [29–37]. However, to the authors' best knowledge, a very limited number of studies have been studied the effect of return fines embedding on the sintering behavior of VTM ore. In this paper, the influence of the particle size range, mass ratio of the return fines, and the height of the embedding layer on productivity, yield, flame front speed, and permeability of sinter packed bed in the sintering process was studied. Moreover, various metallurgical properties, e.g., tumble strength (TI), of the VTM sinter were also evaluated after the sintering process.

2. Materials and Methods

2.1. Raw Materials

Raw materials, i.e., VTM, return fines, quick-lime, limestone, and coke breeze, are from a Chinese sinter plant. The chemical composition of the VTM, return fines, quick-lime and limestone is reported in Table 1. One proximate analysis was also made for the coke breeze shown in Table 2. The blending ratio of the sinter mixture used in the sinter pot experiment is illustrated in Table 3. The basicity (calculated by wt.% CaO/wt.% SiO₂) of the

sinter is kept at 2.34. During the laboratory sinter pot tests, the above two indices (blending ratio and basicity) are carefully chosen based on the referential sinter plant.

Table 1. Chemical composition of part of the raw materials (wt.%).

Materials	TFe	SiO ₂	CaO	MgO	Al ₂ O ₃	S	TiO ₂	V ₂ O ₅	H ₂ O
VTM	54.59	5.42	2.76	2.46	3.11	0.42	6.10	0.50	8.54
Quick-lime	0.50	2.00	87.00	0.81	1.49	0.04			
Limestone	0.50	3.00	28.50	20.50	1.54	1.00			3.00
Return fines	48.48	5.59	13.08	3.18	3.24	0.12	5.40	0.45	

Table 2. Chemical composition of the coke breeze and its ash (wt.%).

Fixed Carbon	Total Sulfur	Volatile	Ash (14.30)						Σ
			FeO	SiO ₂	CaO	MgO	Al ₂ O ₃	Others	
84.00	0.8	1.21	1.16	100	1.15	0.34	4.30	0.02	100

Table 3. Blending ratio of the sinter mixture used in the experiments.

Raw Materials	VTM	Quick-Lime	Limestone	Coke Breeze	Return Fines
wt.%	52.85	5.85	2.40	3.90	35.00

A schematic diagram of return fines embedding technology is shown in Figure 1. The sintering experiment includes proportioning, mixing, granulation, ignition, sintering, cooling, breaking, and screening process, which can simulate the sinter production process in the practical sinter plant. Before the experiment, the raw materials were dried at 105 °C in an oven for two hours. The size distribution of the returned ore is determined by the vibrate screen, and the returned fines with particle size smaller than 3 mm were thoroughly blended with other raw materials. A proper amount of water was added to preheat the mixture. After two minutes, placing the mixture into a cylinder mixer (H (800 mm) × ID (600 mm)) for 5 min to granulate at a rotation speed of 29 r/min. During the granulation period, an appropriate amount of water (7.5% ± 0.1%) was sprayed on the mixture. After granulation, the returned fines with particle size larger than 3 mm are added to the cylinder mixer to mix with already granulated granules 15 s. Finally, the mixture was charged into the sinter pot (ID (300 mm) × H (600mm)). Before the sintering process, 2 kg sinters with the particle size range of 10~14 mm were selected as bedding materials. The sintering mixture was ignited at 1050 °C for 2 min while the suction pressure is 8 kPa. However, the suction pressure was increased to 15 kPa during the sintering process. The experimental conditions are fixed during the experiments, which are reported in Table 4.

Table 4. Experimental conditions of the sintering pot test.

Item	Parameter	Item	Parameter	Item	Parameter
Sinter bed depth	600 mm	Sintering pot diameter	300 mm	Granulation time	7 min
Ignition vacuum	8 kpa	Sintering vacuum	15 kpa	Ignition time	2 min
Ignition temperature	1273 K	Moisture	7.5 ± 0.1 %	Basicity (R = CaO/SiO ₂)	2.34

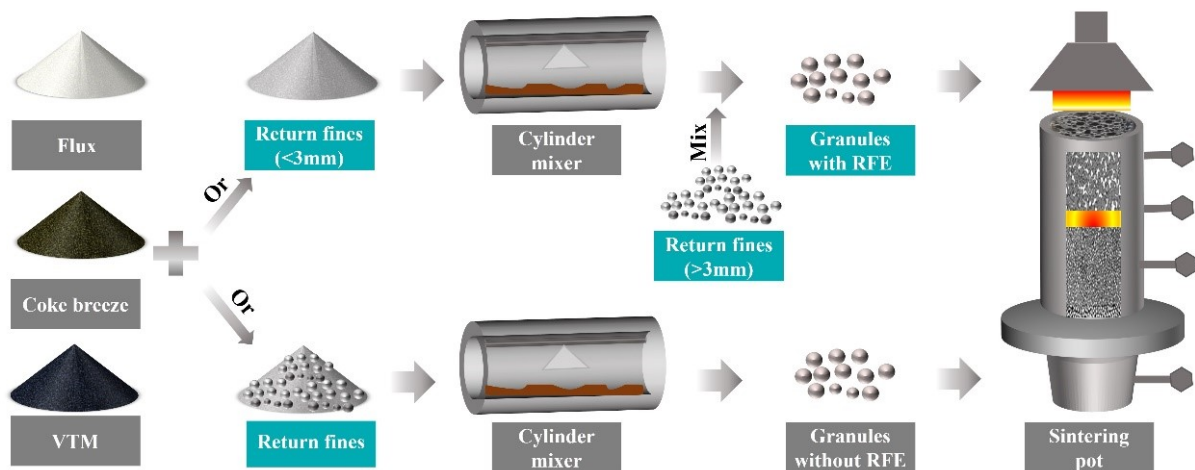


Figure 1. The schematic diagram of return fines embedding technology.

2.2. Metallurgical Characterization of VTM Sinter

Flame front speed (*FFS*), yield (*Y*), productivity (*P*), and tumbler index (*TI*) are calculated Equations (1)–(4) to evaluate the metallurgical properties of the VTM sinter.

$$FFS = H/T, \quad (1)$$

$$Y = (M - M_R)/T \quad (2)$$

$$P = (M \times Y)/(S \times T/60) \quad (3)$$

$$TI = M_T/M_P \quad (4)$$

where *H* is the thickness of the sintering bed (mm), *T* is the sintering time (min), *M* is the mass of the sinter cake (t), *M_R* is the mass of return fines (t), *S* is the cross-sectional area of sinter pot (m²), *M_P* is the mass of the sinters used for the test portion as weighed out and placed in the tumble drum (kg), and *M_T* is the mass of sinters with size + 6.3 mm in the tumble test portion.

TI was measured according to ISO 3271-2015. The sinter with four sizes were obtained separately by sieving the crushed sinters with 40.0 mm, 25 mm, 16 mm, and 10 mm sieves. A 15-kg test sinter was selected from the four sizes sinter according to the proportion of each of the 4 sieves. The sinter was rotated in a circular drum at a speed of 25 r/min for 200 circles. The rotating sample is sieved using a test sieve with 6.3 mm square hole. After the tumble test, the sinter with sizes greater than 6.3 mm was weighed and recorded to calculate the tumble index that is defined as the percentage of finished composite sinter with a particle size greater than 6.3 mm in the overall sinter.

2.3. Permeability

The permeability of the wet granular packed bed was measured in Japanese permeability units (*JPU*) [26]. The sintering mixture permeability was determined according to the Voice formula

$$JPU = (Q/A) \times (H/\Delta P)^{0.6} \quad (5)$$

where *Q* is the airflow rate (m³·min^{−1}), *H* and *A* are the bed height (mm) and the cross-sectional area (m²) of the bed, respectively, and ΔP is the measured pressure drop across the bed (mm H₂O). Notably, the permeability experiment was conducted in a sintering pot (ID (100 mm) × H (500 mm)) as shown in Figure 2. Meanwhile, the parameter of this sintering pot test is exactly the same as those mentioned in the previous section.

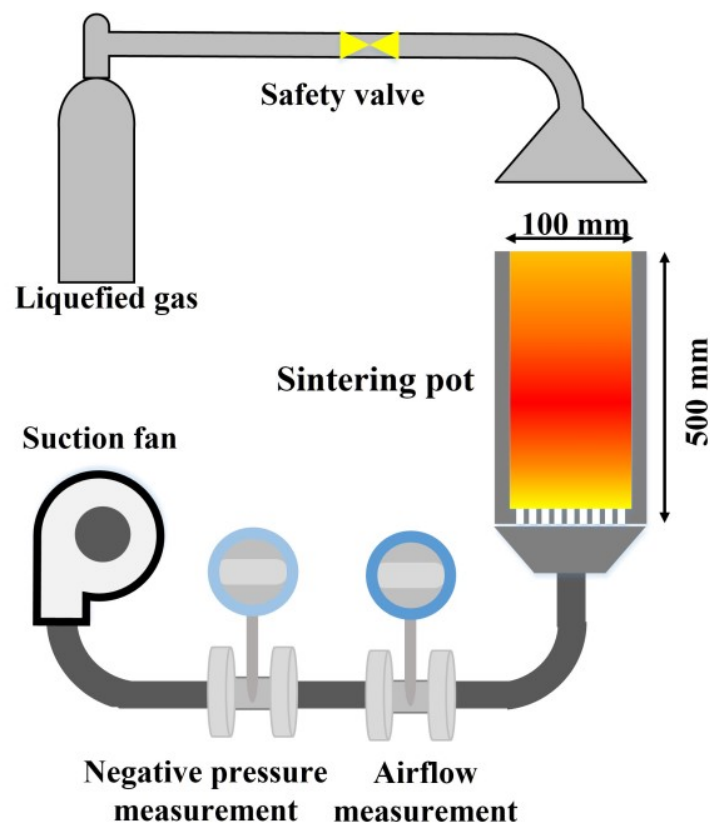


Figure 2. The schematic diagram of the permeability experimental device.

3. Results

3.1. Effect of Particle Size Range of Return Fines for Embedding

To optimize the size of return fines (used for embedding) for effectively improving the permeability of the sinter packer bed, the returned fines were divided into five groups according to their sizes: <1 mm, 1~3 mm, 3~5 mm, 5~7 mm and >7 mm. The above returned fines in five groups were used for five groups embedding experiments separately.

The effect of particle size of return fines for embedding on the productivity, yield, flame front speed, tumble index and particle size distribution of VTM sinter is described in Figures 3 and 4. Figure 3 shows the productivity, yield, flame front speed, and tumble index presenting an increasing trend firstly, then slightly decreasing with the return fine embedded. While it also indicates the four sintering indices are improved clearly generally after introducing the return fines embedding technology in the sintering process, especially for the case with the return fine size 3~5 mm. The productivity, yield, flame front speed, and tumble index are enhanced from $1.15 \text{ t}\cdot\text{m}^{-2}\cdot\text{h}^{-1}$ to $2.19 \text{ t}\cdot\text{m}^{-2}\cdot\text{h}^{-1}$, 70.5% to 80%, $16.96 \text{ mm}/\text{min}^{-1}$ to $24.92 \text{ mm}/\text{min}^{-1}$, and 62.67% to 67.33%, respectively, after using the return fines with size of 3~5 mm. For the above four sintering parameters, FFS is a vitally valuable index for the sintering process since it characterizes the permeability of the sinter packed bed. In general, a higher FFS means a higher sinter bed permeability which is conducive to shorten the sintering time. The productivity and FFS of the VTM sinter reach their peak together, which can be attributed to a higher FFS meaning less sintering time, which can also improve the productivity. Thus, one optimized return fine size is 3~5 mm for embedding, which can keep high permeability of sinter packed bed. In addition, compared to the base sample, when the size range of the embedding return fines is <1 mm, both TI and yield of the sinter are decreased. This may be due to the fact that the size of the return fines used for embedding is too small and the mixing time at the end without granulation is only 15 s. This causes deplorable granulation performance and further affects the strength and size distribution of sinter, finally resulting in its yield reduction. There are two main

reasons for the improvement in the permeability of the sinter packed bed. Firstly, with the implementation of the return fines embedding technology, voids are created around the large size return fines to improve the permeability of the sinter packed bed [24]. Then, during the usual granulation process, the large size return fines may crush the smaller granules, resulting in a deterioration of the granulation performance. The granulation performance is improved by the implementation of the return fines embedding technology.

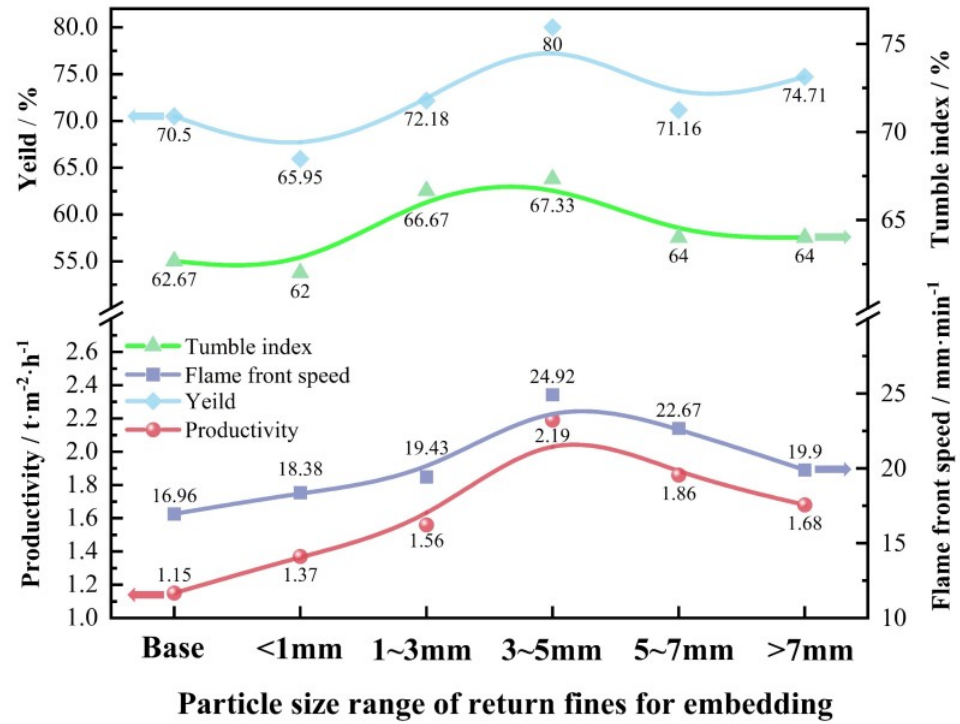


Figure 3. Effect of particle size of return fines for embedding on VTM sintering indices.

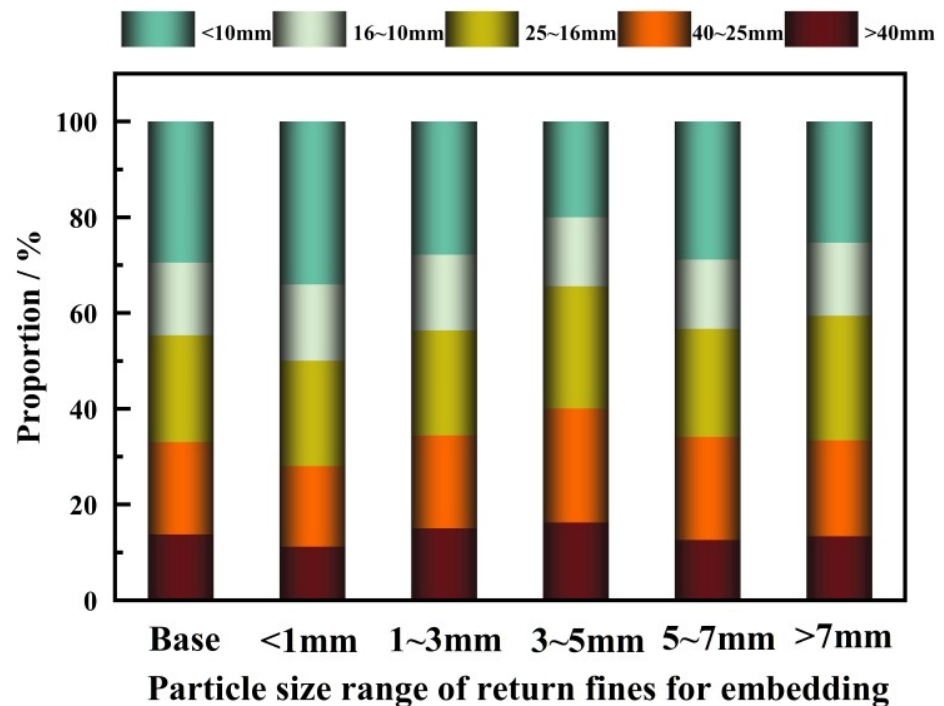


Figure 4. Effect of particle size of return fines for embedding on VTM sinter size distribution.

As shown in Figure 4, the size of the return fines for embedding had little effect on the size distribution of the vanadium and titanium sinter. However, at return fines for embedding size less than 1mm, the largest proportion of sinter size less than 10, and therefore the lowest yield, is achieved, consistent with that mentioned previously.

3.2. Effect of Mass Ratio of Return Fines for Embedding

Similarly, to identify the optimal mass ratio of return fines for embedding, the return fines (greater than 3 mm) were made to mix directly without granulation. The specific experimental scheme is shown in Table 5. The effect of mass ratio of return fines used for embedding on VTM sinter productivity, yield, flame front speed, tumble index, and sinter particle size distribution is shown in Figures 5 and 6. It has been observed that the productivity and FFS of the VTM sintering process show an increasing trend as the mass ratio of return fines for embedding increases from 20% to 80%. At the same time, the TI of VTM sinter continue to decline, probably because a reduction of sintering time can lead to insufficient sintering reaction time, which affects the quality of the sinter. However, when the mass ratio exceeds 80%, there is a noticeable deterioration in all the four indices, i.e., productivity, yield, FFS, and TI. During the granulation of the raw material, the returned fines will act as the central nucleus of the particles to bond the fines with water to generate granules. According to the blending ratio, a total of 28 kg of return fines was involved in the granulation. Compared to the base sample without returned fines embedding, 13.65 kg of embedding was not involved in the granulation when the proportion of returned fines was 100%, resulting in a reduction of approximately 8% in the total mass of fines involved in granulation. This would result in a lack of the amount of central nucleus in the granulation process. The finer powders cannot be cemented into granules due to insufficient central nucleus, which finally leads to insufficient granules and further contributes to inferior granulation properties and sintering indices. As shown in Figure 6, the size of the return fines used for embedding has a considerable effect on the size distribution of the VTM sinter. At a 20% embedding mass ratio, the smallest proportion of sinter larger than 10 mm and the largest proportion of sinter smaller than 10 mm are found. At an 80% embedding mass ratio, the size distribution of sinter is greatest for 16–25 mm and smallest for sizes less than 10 mm. In the end, the optimum mass ratio of return fines for embedding in the VTM sintering process is 80%.

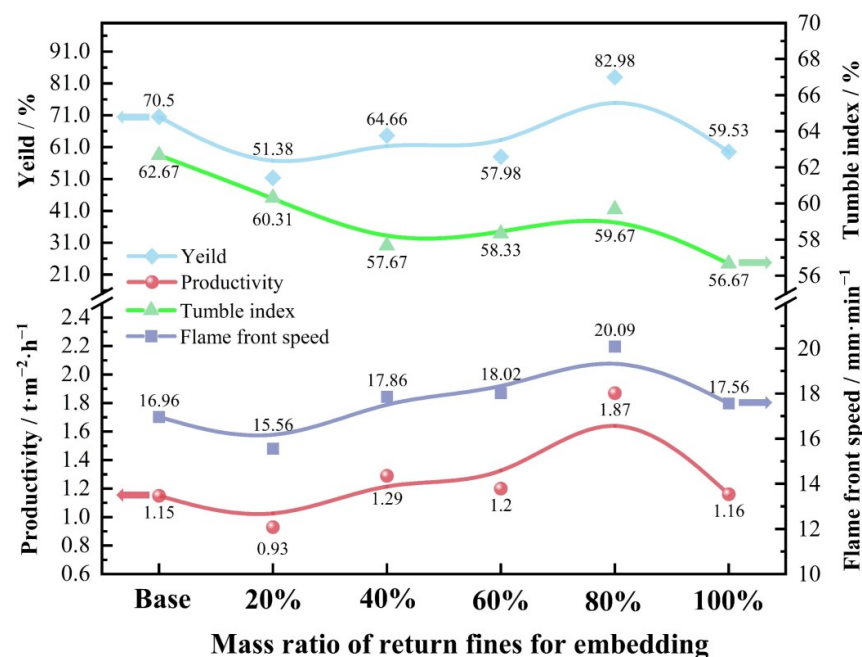


Figure 5. Effect of mass ratio of return fines for embedding on VTM sintering indices.

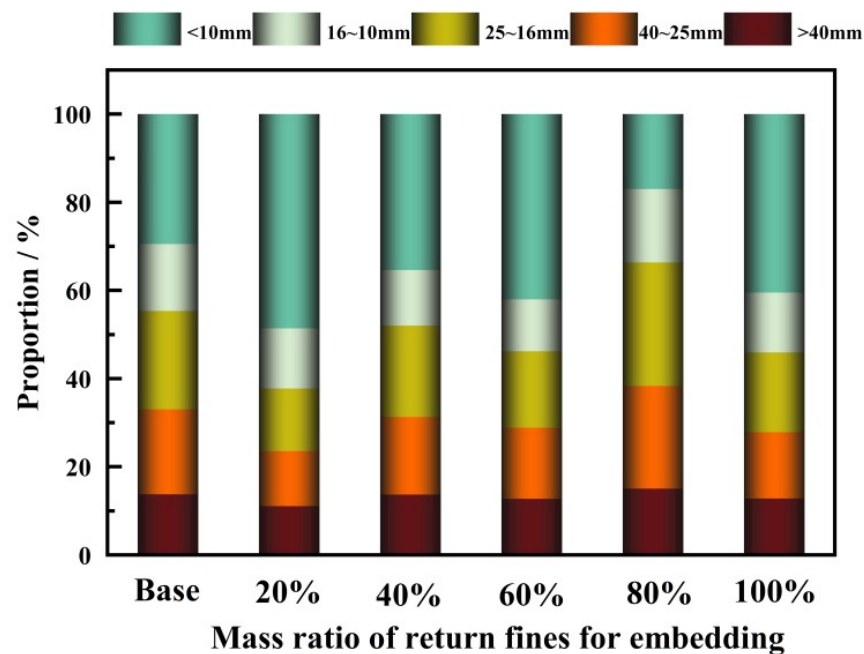


Figure 6. Effect of mass ratio of return fines for embedding on VTM sinter particle size distribution.

Table 5. Experimental scheme for mass ratio of return fines (>3 mm) used as embedding.

Mass Ratio/%	20	40	60	80	100
Embedding mass/kg	2.73	5.46	8.19	10.92	13.65

3.3. Effect of Layer Location of Return Fines for Embedding

In the previous section, the effect of particle size range and mass ratio of return fines for embedding on the VTM sintering process was discussed. In this section, discussion focuses mainly on the effect of the layer location of the return fines used for embedding. The sintering pot was divided into three separate height layers (shown in Figure 7), and the return fines can be placed in one or two of them, as illustrated in Figure 7.

As shown in Figures 8 and 9, among the five different locations of embedded return fines, the FFS and productivity are the lowest if the return fines are located in the upper layer, which could be due to the fact that the upper layer of the sintering pot is situated in the upper location, and the improvement in the permeability of the upper layer is insufficient to provide an adequate enhancement in the permeability of the entire sinter packed bed. In addition to this, embedding in the upper layer fails to rectify the impact of the over-wet zone in the lower part of the sintering pot on the permeability [38,39], leading to excessive sintering time and low FFS. At the same time, the productivity and FFS are higher for the case with embedded return fines in the lower (or middle + lower) layer compared to placing the return fines in the upper layer. On the one hand, the elevation of the FFS demonstrated once again that the permeability of the sinter packed bed is improved by the return fines embedding technology. On the other hand, it indicates the serious deterioration of the sinter packed bed permeability in the bottom part of the sinter pot due to moisture migration from the over-wet zone. In general, the middle-lower layer is the most compatible location for return fines embedding during the VTM sintering process. As shown in Figure 9, the location of the return fines used for embedding had practically no influence on the size distribution of the VTM sinter.

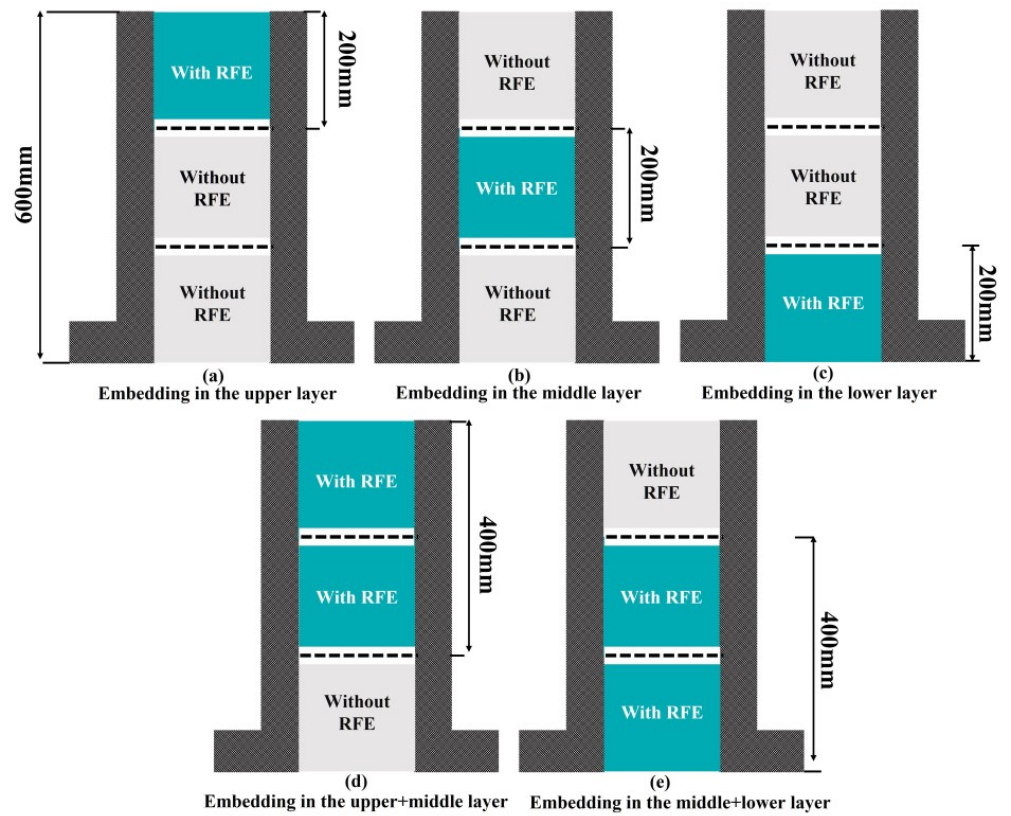


Figure 7. Different possible embedded locations of the return fine layer in the sinter pot: (a) upper layer, (b) middle layer, (c) lower layer, (d) upper + middle layers, and (e) middle + lower layers.

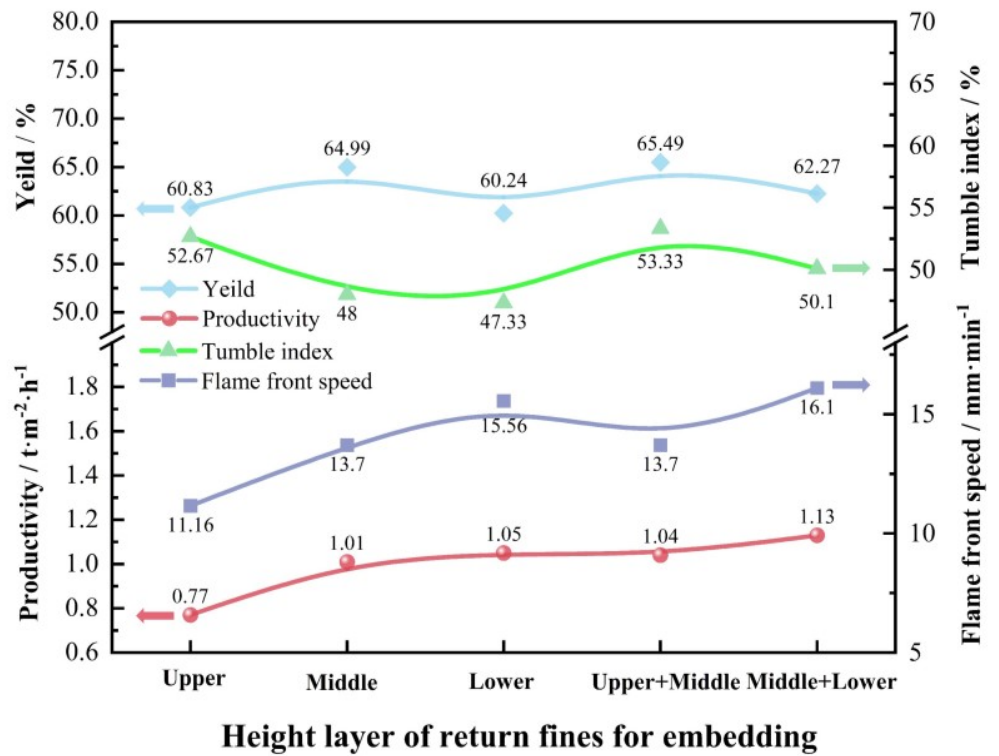


Figure 8. Effect of location of return fines for embedding on VTM sintering indices.

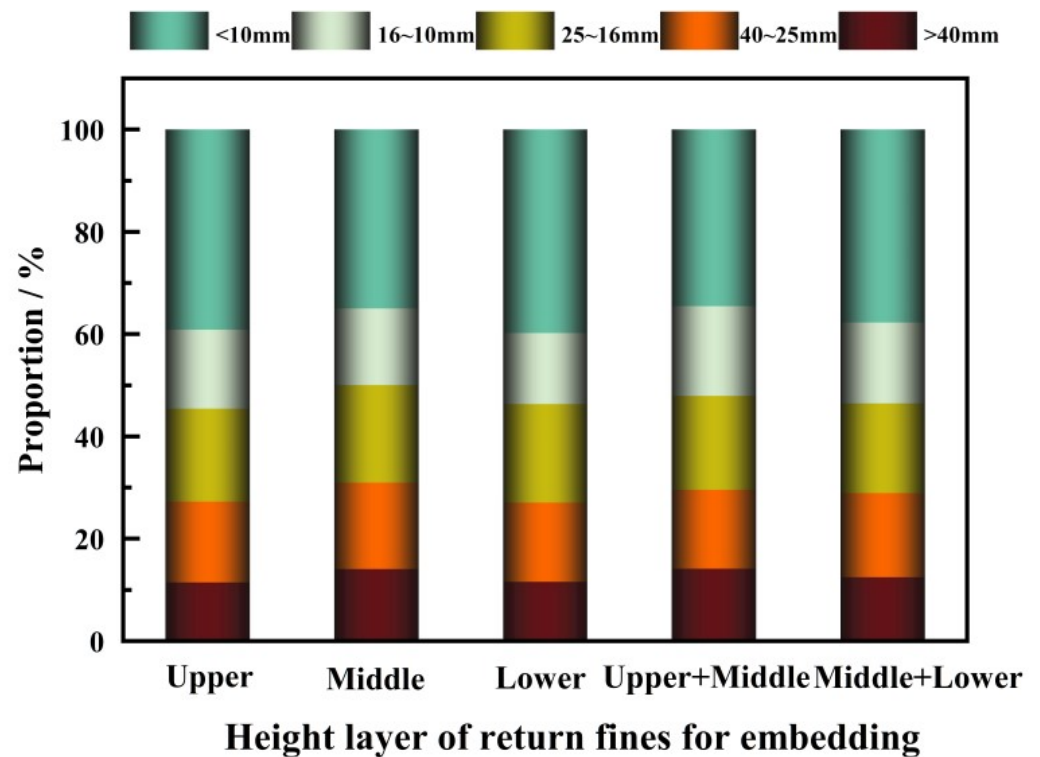


Figure 9. Effect of location of return fines for embedding on the particle size distribution of VTM sinter.

3.4. Effect of Mass Ratio of Return Fines for Embedding on Sinter Bed Permeability

In order to demonstrate the effect of return fines embedding technology on the permeability of sinter packed bed straightforwardly, the permeability of sinter packed bed have been tested directly for some experiments, which can also help to validate part of the previous experimental results. This section mainly investigates the effect of the mass ratio of return fines for embedding on the permeability of the sinter packed bed. The experiments were carried out on the sinter pot (ID (100 mm) × H (500 mm)) with a charge of 10 kg sinter raw materials and the same return fines are also used here.

The experimental results are shown in Figure 10. It illustrates that as the mass ratio of return fines increases from 0 to 50%, the permeability of the sinter packed bed increases from 21.24 JPU to 26.37 JPU at the start of sintering process. During the sintering process of VTM, the permeability of the sinter packed bed undergoes two major increases. The increase in the permeability of the sinter packed bed for the first time was due to the fact that the negative pressure at the ignition was 8 kp and after the ignition the negative sinter pressure increased to 15 kp. As the negative pressure increased the air flow through the sinter pots also increased and the permeability of the sinter packed bed was increased according to Equation (5). Then, the permeability remains in a relatively stable condition until the sintering reaches the later stage. At this stage, the permeability raises rapidly and reaches the peak near the termination of sintering. Figure 10 also describes that as the mass ratio of return fines for embedding increases, the permeability of the sinter packed bed almost enhances at each stage of sintering. This implies a reduction in sintering time and an increase in FFS, which is identical to the findings in the previous section.

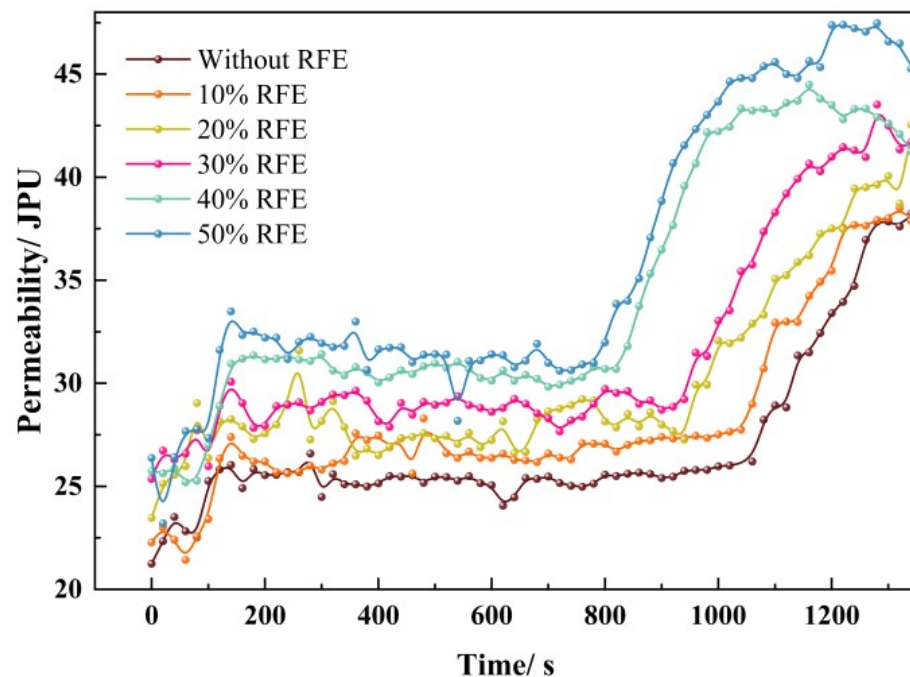


Figure 10. Effect of the mass ratio of return fines for embedding on the permeability of the sinter packed bed.

4. Conclusions

In this paper, through sintering pot tests, the influence of the return fines particle size, mass ratio, and embedded location on productivity, yield, flame front speed, and permeability of sinter packed bed in the sintering process was clarified. The main conclusions are as follows.

- (1) The productivity, yield, flame front speed, and tumble index of the VTM sintering process are all increased to a certain extent after embedding different sizes of returned fines. Most notably, the optimal productivity, yield, flame front speed, and tumble index occur when the particle size of return fines for embedding is 3~5 mm.
- (2) The optimal mass ratio of return fines for embedding was confirmed at 80%, due to its FFS reaching $20.09 \text{ mm}/\text{min}^{-1}$, which is the most favourable mass ratios. A continued increase in the mass ratio results in a decrease in FFS, yield, productivity, and TI.
- (3) Among the five different possible locations of embedded return fine layer, the middle-lower layer corresponds to the highest FFS. By contrast, using the upper layer as the embedded layer, both FFS and productivity reach minima.
- (4) As the mass ratio of return fines for embedding enhances from 0% to 50%, the permeability of the sinter packed bed is improved at each stage of sintering. In addition, the time taken for permeability to peak consequently shortens, which implies a reduction in sintering time and an increase in FFS.

Author Contributions: Conceptualization, H.L. and Y.Q.; methodology, H.L., F.M.; investigation, S.P., Z.S. and H.H.; writing—original draft preparation, S.P.; writing—review and editing, W.L., G.W. and Y.Q. All authors have read and agreed to the published version of the manuscript.

Funding: This research was funded by the Natural Sciences Foundation of Chongqing, China (No. cstc2021ycjh-bgzxm0211), Graduate Science and Technology Innovation Project of Chongqing University of Science and Technology (No. YKJCX2120215).

Institutional Review Board Statement: The study did not require ethical approval.

Informed Consent Statement: Not applicable.

Data Availability Statement: Not applicable.

Acknowledgments: We strongly appreciated the support and assistance of Longhai Liu and Baisun Yang of Sichuan Desheng Group Vanadium and Titanium Limited for their contribution to this publication.

Conflicts of Interest: The authors declare no conflict of interest.

References

1. Zhang, S.; Liu, S.; Ma, W.; Zhu, K.; Cao, L.; Dai, Y. Present Status and Development of Comprehensive Utilization of Vanadium-Titanium Magnetite. *Rare Met. Technol.* **2017**, *2017*, 203–210.
2. Zhou, M.; Zhou, H.; O’dea, D.P.; Ellis, B.G.; Honeyands, T.; Guo, X. Characterization of Granule Structure and Packed Bed Properties of Iron Ore Sinter Feeds that Contain Concentrate. *ISIJ Int.* **2017**, *57*, 1004–1011. [[CrossRef](#)]
3. Zhou, M.; Xu, J.; Zhou, H. Evaluating the permeability properties of green bed in iron ore sintering using high resolution X-ray computed tomography and orthogonal array tests. *Powder Technol.* **2020**, *375*, 360–368. [[CrossRef](#)]
4. Lu, Y.; Wu, S.; Niu, L.; Liu, Z.; Zhou, H.; Hong, Z.; Song, S. Treatment of vanadium–titanium magnetite based on composite agglomeration process (CAP). *Ironmak. Steelmak.* **2020**, *48*, 477–482. [[CrossRef](#)]
5. Ax, K.; Feise, H.; Sochon, R.; Hounslow, M.; Salman, A. Influence of liquid binder dispersion on agglomeration in an intensive mixer. *Powder Technol.* **2008**, *179*, 190–194. [[CrossRef](#)]
6. Gong, S.; Zuo, Z.; Xie, G.; Lu, H.; Zhang, J. Numerical simulation of wet particle flows in an intensive mixer. *Powder Technol.* **2019**, *346*, 301–315. [[CrossRef](#)]
7. You, Y.; Guo, J.; Lv, X.; Wu, S.; Li, Y.; Tang, K.; Yu, Y. Numerical Simulation of Particle Mixing Behavior in High Speed Shear Mixer and Cylinder Mixer. *ISIJ Int.* **2021**, *61*, 2059–2065. [[CrossRef](#)]
8. Ji, Z.; Zhang, Y.; Gan, M.; Fan, X.; Chen, X.; Huang, X. Importance of intensive mixing on sintering with fine-grained iron ore materials: Characterization and function mechanism. *J. Mater. Res. Technol.* **2020**, *9*, 14443–14453. [[CrossRef](#)]
9. Yang, C.; Zhu, D.; Pan, J.; Lu, L. Granulation Effectiveness of Iron Ore Sinter Feeds: Effect of Ore Properties. *ISIJ Int.* **2018**, *58*, 1427–1436. [[CrossRef](#)]
10. You, Y.; Guo, J.; Li, G.; Lv, X.; Wu, S.; Li, Y.; Yang, R. Investigation the iron ore fine granulation effects and particle adhesion behavior in a horizontal high-shear granulator. *Powder Technol.* **2021**, *394*, 162–170. [[CrossRef](#)]
11. Tardos, G.I. Critical parameters and limiting conditions in binder granulation. *Powder Technol.* **1997**, *94*, 245–258. [[CrossRef](#)]
12. Linhares, F.M.; Victor, C.C.F.; Lemos, L.R.; Bagatini, M.C. Effect of three different binders and pellet feed on granulation behaviour of sintering mixtures. *Ironmak. Steelmak.* **2019**, *47*, 991–997. [[CrossRef](#)]
13. Zhang, F.; Zhu, D.-Q.; Pan, J.; Mo, Y.-P.; Guo, Z.-Q. Improving the sintering performance of blends containing Canadian specularite concentrate by modifying the binding medium. *Int. J. Miner. Metall. Mater.* **2018**, *25*, 598–608. [[CrossRef](#)]
14. Zhou, H.; Zhou, M.; O’dea, D.P.; Ellis, B.G.; Chen, J.; Cheng, M. Influence of Binder Dosage on Granule Structure and Packed Bed Properties in Iron Ore Sintering Process. *ISIJ Int.* **2016**, *56*, 1920–1928. [[CrossRef](#)]
15. Nandy, B.; Chaudhury, M.K.; Paul, J.; Bhattacharjee, D. Sintering Characteristics of Indian Chrome Ore Fines. *Metall. Mater. Trans. B* **2009**, *40*, 662–675. [[CrossRef](#)]
16. Roshan, V.; Kumar, K.; Kumar, R.; Nageswara Rao, G.V.S. Preparation of Iron Ore Micro-pellets and Their Effect on Sinter Bed Permeability. *Trans. Indian Inst. Met.* **2018**, *71*, 2157–2164. [[CrossRef](#)]
17. Lv, X.W.; Bai, C.G.; Zhou, C.Q.; Xie, H.; Shi, R.M. New method to determine optimum water content for iron ore granulation. *Ironmak. Steelmak.* **2013**, *37*, 407–413. [[CrossRef](#)]
18. Higuchi, T.; Lu, L.; Kasai, E.; Yamamoto, T.; Matsuno, H. Inter–particle water infiltration dynamics of iron ore fines during granulation process. *Powder Technol.* **2018**, *339*, 550–559. [[CrossRef](#)]
19. Litster, J.D. Influence of the Material Properties of iron Ore Sinter Feed on Granulation Effectiveness. *Powder Technol.* **1988**, *55*, 144–151. [[CrossRef](#)]
20. Otsu, T.; Nakamura, H.; Ohsaki, S.; Watano, S.; Fujiwara, S.; Higuchi, T. Determining Optimum Water Content for Iron Ore Granulation using Agitation Torque of Wet Ore Powder. *ISIJ Int.* **2022**, *62*, 1381–1388. [[CrossRef](#)]
21. Zhu, D.; Guo, Z.; Pan, J.; Zhang, F. A study of pre-briquetting granulation sintering of the mixtures with high ratio of Brazilian specularite concentrate. *Ironmak. Steelmak.* **2016**, *43*, 721–729. [[CrossRef](#)]
22. Zhou, H.; Lai, Z.; Lv, L.; Fang, H.; Meng, H.; Zhou, M.; Cen, K. Improvement in the permeability of sintering beds by drying treatment after granulating sinter raw materials containing concentrates. *Adv. Powder Technol.* **2020**, *31*, 3297–3306. [[CrossRef](#)]
23. Huang, X.; Lv, X.; Bai, C.; Qiu, G.; Lu, L. Effect of Pre-wetting Treatment on the Granulation Behavior of Iron Ore Fines. *ISIJ Int.* **2014**, *54*, 2721–2727. [[CrossRef](#)]
24. Kasai, E. Design of Bed Structure Aiming the Control of Void Structure Formed in the Sinter Cake. *ISIJ Int.* **2005**, *45*, 535–543. [[CrossRef](#)]
25. Kasai, E. Heat Transfer Analysis of the Mosaic Embedding Iron Ore Sintering (MEBIOS) Process. *ISIJ Int.* **2009**, *49*, 681–686.
26. Matsumura, M.; Yamaguchi, Y.; Hara, M.; Kamijo, C.; Kawaguchi, T.; Nakagawa, Y. Improvement of Sinter Productivity by Adding Return Fine on Raw Materials after Granulation Stage. *ISIJ Int.* **2013**, *53*, 34–40. [[CrossRef](#)]
27. Wang, Z. Study on process of strengthening granulation based on sinter returns and BF returns shunting. *Sinter. Pelletizing* **2018**, *43*, 12–16.

28. Liu, J. Research on MEBIOS technology of different particle sizes and its application. *Sinter. Pelletizing* **2020**, *45*, 22–26.
29. Yang, S.; Tang, W.; Zhou, M.; Jiang, T.; Xue, X.; Zhang, W. Effects of Dolomite on Mineral Compositions and Metallurgical Properties of Chromium-Bearing Vanadium–Titanium Magnetite Sinter. *Minerals* **2017**, *7*, 210. [[CrossRef](#)]
30. Zhou, M.; Yang, S.T.; Jiang, T.; Xue, X.X. Influence of MgO in form of magnesite on properties and mineralogy of high chromium, vanadium, titanium magnetite sinters. *Ironmak. Steelmak.* **2014**, *42*, 217–225. [[CrossRef](#)]
31. Zhang, L.; Yang, S.; Tang, W.; Yang, H.; Xue, X. Effect of coke breeze content on sintering mechanism and metallurgical properties of high-chromium vanadium-titanium magnetite. *Ironmak. Steelmak.* **2019**, *47*, 821–827. [[CrossRef](#)]
32. Zhang, L.; Gao, Z.; Yang, S.; Tang, W.; Xue, X. Effect of Basicity on Sintering Behavior and Metallurgical Properties of High-Chromium Vanadium-Titanium Magnetite. *Metals* **2020**, *10*, 569. [[CrossRef](#)]
33. Zhou, M.; Yang, S.-T.; Jiang, T.; Zhang, L.-H.; Xiao, J.-T.; Xue, X.; Zhang, W.-J. Effects of carbon content on the sintering behavior of low-titanium vanadium-titanium magnetite. *Metall. Res. Technol.* **2016**, *113*, 612. [[CrossRef](#)]
34. Tang, W.-D.; Yang, S.-T.; Zhang, L.-H.; Huang, Z.; Yang, H.; Xue, X.-X. Effects of basicity and temperature on mineralogy and reduction behaviors of high-chromium vanadium-titanium magnetite sinters. *J. Cent. South Univ.* **2019**, *26*, 132–145. [[CrossRef](#)]
35. Li, G.; Lv, X.; Zheng, Z.; Ling, J.; Qiu, G. Effect of Preformed Calcium Ferrite Addition on Sintering Behavior of Vanadium Titanium Magnetite Ore. *JOM* **2020**, *73*, 316–325. [[CrossRef](#)]
36. Yang, S.; Zhou, M.; Jiang, T.; Xue, X. Study on Sintering Characteristics of Ultra-Poor Vanadium-Titanium Magnetite. *Minerals* **2021**, *11*, 515. [[CrossRef](#)]
37. Zhou, M.; Jiang, T.; Yang, S.-T.; Xue, X.-X. Sintering behaviors and consolidation mechanism of high-chromium vanadium and titanium magnetite fines. *Int. J. Miner. Metall. Mater.* **2015**, *22*, 917–925. [[CrossRef](#)]
38. Han, H.; Lu, L. Recent advances in sintering with high proportions of magnetite concentrates. *Miner. Process. Extr. Metall. Rev.* **2017**, *39*, 217–230. [[CrossRef](#)]
39. Zhou, H.; Ma, P.; Cheng, M.; Zhou, M.; Li, Y. Effects of Temperature and Circulating Flue Gas Components on Combustion and NO_x Emissions Characteristics of Four Types Quasi-particles in Iron Ore Sintering Process. *ISIJ Int.* **2018**, *58*, 1650–1658. [[CrossRef](#)]

Disclaimer/Publisher’s Note: The statements, opinions and data contained in all publications are solely those of the individual author(s) and contributor(s) and not of MDPI and/or the editor(s). MDPI and/or the editor(s) disclaim responsibility for any injury to people or property resulting from any ideas, methods, instructions or products referred to in the content.